3D In-situ XCT Image Based Meso-scale Fracture Modelling and Validation of Concrete Using Voxel Hexahedron Meshing and Damage Plasticity Model

Yujie Huang[1], Zhenjun Yang[1,2*], Wenyuan Ren[2], Guohua Liu[1], Chuanzeng Zhang[3]

[1]College of Civil Engineering and Architecture, Zhejiang University, 310058, China.
[2]School of Mechanical, Aerospace and Civil Engineering, the University of Manchester, M13 9PL, UK.
[3]Department of Civil Engineering, University of Siegen, Paul-Bonatz-Str. 9-11, D-57076 Siegen, Germany

*Corresponding author: zhjyang@zju.edu.cn

Abstract

Three-dimensional (3D) meso-scale finite element models of concrete in compression based on in-situ X-ray Computed Tomography (XCT) images are developed and validated in this study. The micro-scale images from a Brazilian-like in-situ XCT test are first compressed and then transformed into manageable meso-scale 3D meshes using a voxel hexahedron meshing technique with a stacking algorithm. The concrete damaged plasticity model in ABAQUS is used to simulate complicated damage and fracture behaviour of concrete. Excellent qualitative agreement is found between the simulations and the XCT test in terms of damage evolution and fracture process on both the surface and interior of the specimen. The effects of internal heterogeneous meso-structures on the macro-scale loading-carrying capacities and failure patterns are quantitatively and qualitatively evaluated by modelling different uniaxial loading directions.

Keywords: Concrete in compression, In-situ X-ray computed tomography, Voxel hexahedron meshing, 3D Image based modelling, Concrete damage plasticity model, Finite element method

1. Introduction

Traditional concrete fracture models assuming homogeneous material properties often predict unrealistically smooth or wrong crack paths and load-carrying capacity of unknown reliability due to its multi-phase, heterogeneous internal structures at micro/meso-scales [Yang and Xu (2008)]. It is highly necessary to conduct micro/meso-scale modelling for accurate understanding of complex damage initiation and evolution until failure, and the relationships between physical properties of multi-phases and the macro-scale mechanical responses [López et al. (2008)].

As to meso-scale modelling, the meso-structures can be directly represented by different phases artificially generated and randomly distributed in space [Caballero et al. (2006); López et al. (2008) Yin et al. (2013)], or be indirectly modelled by random fields satisfying certain correlation functions describing heterogeneous material properties [Yang and Xu (2008); Yang et al. (2009); Su et al. (2010)]. However, most of these studies use assumed meso-scale morphologies or random fields that are not the same as the real internal structures so that the numerical models cannot be directly validated. In addition, most of the existing studies are in 2D and cannot predict non-planar 3D fracture surfaces in reality. Consequently, the simulated results may be neither representative nor fully verifiable. This has led to development of numerical models that are converted from images captured by digital cameras and microscopes etc [Young et al. (2008)]. In this way, more accurate micro/meso-structures can be directly simulated.

Recently, the X-ray Computed Tomography (XCT) technique with non-destructive multi-length scale capabilities becomes increasingly popular, mostly to acquire micro/meso-scale internal structures of concrete [Wang et al. (2003)], and occasionally, to observe damage evolution and fracture process using in-situ XCT tests [Yang et al. (2013)]. The XCT-images have been converted

using commercial packages AVIZO and Simpleware to finite element (FE) meshes by the second author's group, for 2D and 3D cohesive fracture modelling with limited success [Ren et al. (2013; 2014)] and 3D homogenization of elastic properties [Sharma et al. (2014)]. However, in the commercial packages, 3D surface contours are extracted from image datasets and then discretised in mesh generation [Canton and Gilchrist (2010)], which often results in many distorted FE elements when large element sizes are used, or otherwise millions of elements that are beyond the power of conventional computers.

In this study we develop a novel 3D XCT-image based meso-scale FE fracture modelling method for concrete under compression, and attempt to validate 3D damage initiation and evolution until failure predicted by the models for the first time. The voxel hexahedron meshing method [Keyak et al. (1993); Hollister et al. (1994); Crawford et al. (2003)] is augmented with image compression and slice stacking algorithms to efficiently generate 3D FE meshes. It avoids the problem of commercial packages and is able to control the mesh density while maintaining the original 3D morphology. The concrete damage plasticity (CDP) model in ABAQUS is used to simulate complicated damage initiation and evolution in concrete under compression. The in-situ XCT test of a concrete cube under Brazilian-like compression [Yang et al. (2013)] is modelled to validate the developed method, followed by detailed investigation of traditional uniaxial compressive tests.

2. XCT-image based hexahedron mesh generation

Most of the existing image-based 3D FE models based on voxel hexahedron meshing are constructed by direct conversion of voxels in digital images to the same-sized cubic finite elements [Hollister et al. (1994)]. They cannot readily adjust element size while faithfully maintaining the original morphology. In this study, a bottom-up algorithm with the following steps is proposed and fully automated in a MATLAB code:

2.1 2D image processing

For each slice of images from the in-situ XCT test [Yang et al. (2013)], there are 372 pixels of 0.1mm in both directions (Figure 1a). The grey value of pixels ranges from 0 to 255 and drastically fluctuates near the phase interfaces. Segmentation is conducted on each slice using proper thresholds, resulting in ternary images with 1 for aggregates, 2 for mortar and 3 for voids (Figure 1a, refer to [Ren et al. (2013)]). To build lower resolution models, the segmented images are compressed by re-building connectivity of aggregate pixels. Adjustment of grey value of a small number of pixels is then carried out to maintain the morphological details. Figure 1b and 1c show the compressed image with 0.2mm and 0.4 mm pixels, respectively.

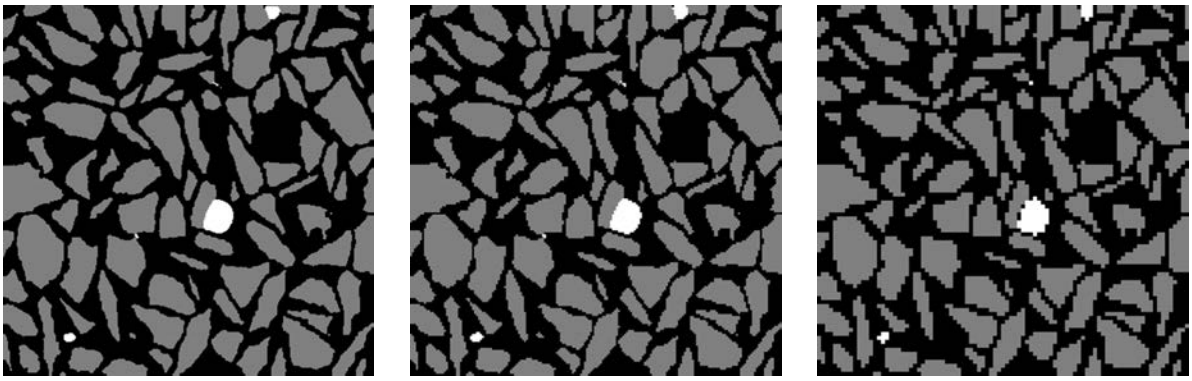

(a) 372×372 pixels (0.1mm) **(b) 186×186 pixels (0.2mm)** **(c) 93×93 pixels (0.4mm)**

Figure 1. Image compression

2.2 Slice stacking

The 2D image slices are then stacked to generate voxels. The stacking algorithm widely used [Terada et al. (1997); Huang and Li (2013)] is adopted here and illustrated in Figure 2. The resultant voxels can be converted into eight-noded hexahedral elements and directly used for modelling inclusions of simple shapes, as in the above existing studies, but not for modelling complicated aggregates and voids in concrete of this study. To maintain the true internal morphology, further operations on the voxels are carried out to avoid cases such as contact between aggregates, mortar inside aggregates etc. Figure 3a and 3b show the resultant morphology of aggregates and mortar, respectively. The initial cracks and voids are shown in Figure 3c.

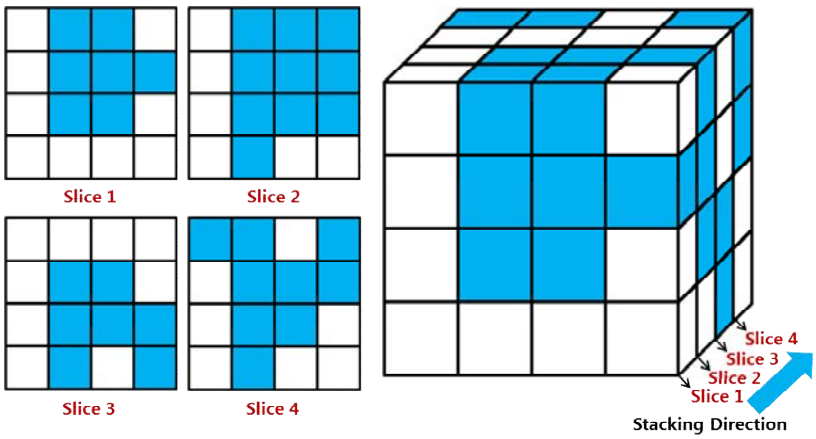

Figure 2. Slice stacking

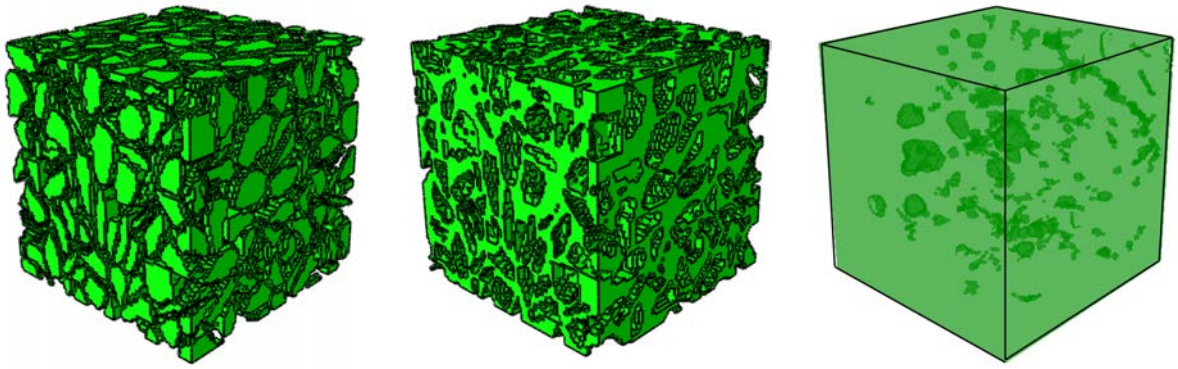

(a) Aggregate **(b) Mortar** **(c) Initial voids and cracks**

Figure 3. 3D meso-scale morphology after slice stacking

2.3 Identification of interfacial transition zone (ITZ)

In this step, the mortar voxels connected with aggregate voxels are identified and used to model the weaker aggregate-mortar interfaces, namely the interfacial transition zone (ITZ). Figure 4 shows a small part of the full model with the ITZs displayed in red as an example. The ITZ thickness is 0.4 mm for the coarsest model and 0.1mm for the finest model, respectively.

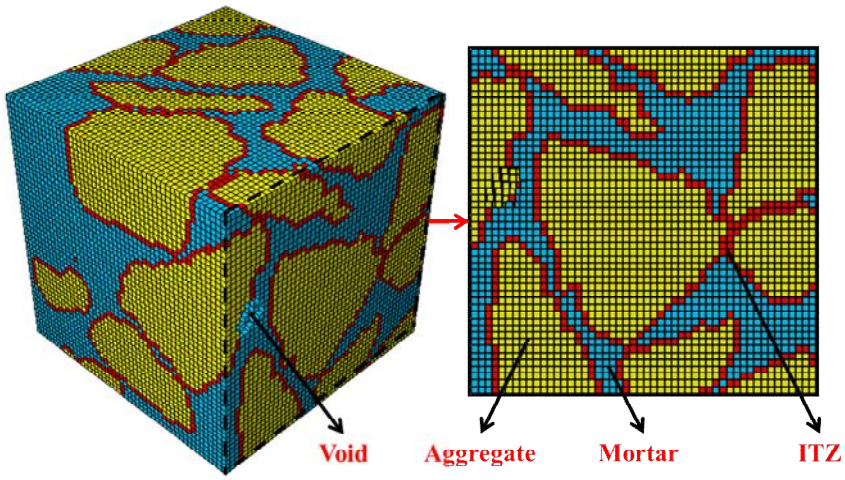

Figure 4. Identification of materials with ITZs

2.4 Generation of 3D FE meshes

After the material labels of all the voxels are determined, the FE meshes are generated by converting each voxel into an eight-noded hexahedral cubic element. Figure 5b shows the final model with ITZ highlighted (the mesh is too dense to be seen clearly), compared with the original XCT image in Figure 5a.

To investigate the effect of image compression and slice stacking, the volume fractions of different phases are calculated. It is 45.755% for aggregates and 1.068% for voids respectively for 0.4mm size model, compared closely with 48.212% and 0.912% respectively for the original 0.1mm size specimen. This suggests that the proposed method is able to maintain the original internal morphology even with 64-time compression of voxel number and thus a nearly 64-time reduction in 3D cubic finite elements.

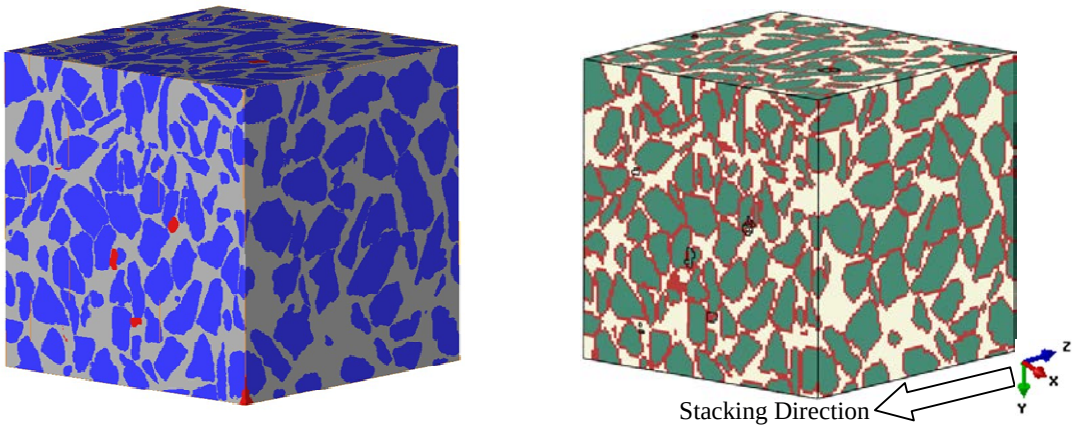

(a) XCT specimen **(b) Numerical model**

Figure 5. Comparison of morphology

3. Numerical Simulations and Validation

3.1 In-situ XCT Test

The in-situ XCT test [Yang et al. (2013)] of a concrete cube is modelled first. The tested concrete cube is 40mm (see Figure 6 below). The compressive loading is applied on a central area of 17.5

mm×17.5 mm on the top face; the bottom face is fixed in the same area. This loading condition is similar to typical Brazilian tests. The voxel resolution in the XCT scans is 37.2 μm.

The uneven surfaces of the 40mm cube are removed to build the 37.2 mm FE model shown in Figure 5b with uniform element size 0.4mm. The model consists of 795,764 cube elements and 837,371 nodes. The loading is applied by uniformly distributed displacements on the loaded area with the maximum displacement 0.186mm or strain 0.005. The ABAQUS/Explicit solver is employed with total time 0.01s to ensure the quasi-static loading condition.

3.2 Material model and parameters

The CDP model in ABAQUS, which has proved very powerful for modelling concrete damage and fracture [Lubliner et al. (1989); Lee and Fenves (1998); Chen et al. (2012); Mahmud et al. (2013)], is used to model mortar and ITZs, and the aggregates are assumed elastic. The compressive strength is 35MPa and 27MPa for mortar and ITZs, respectively. The corresponding tensile strength is 4.5MPa and 3.5MPa, respectively. The stress-strain curves in the 2010 Chinese Code for Design of Concrete Structures are used to model compression and tension. The tensile behaviour is defined by an equivalent stress-displacement curve to ensure mesh independence of results. The Young's modulus is 50GPa, 20GPa and 15GPa for aggregates, mortar and ITZs, respectively. Default values in ABAQUS are used for other parameters of the CDP model.

3.3 Validation of final crack pattern

As the material parameters are not from the in-situ XCT test, only the predicted final crack pattern is validated against the XCT test. Figure 6 compares the failed specimen in the test with predicted macroscopic crack pattern represented by the maximum principal strain on the surface. The crack pattern resembles typical ones in Brazilian tests [Lopez et al. (2008)]. Figure 7 compares the crack paths with respect to the aggregates on the surface in a different view from Figure 6. Figure 8 compares the internal voids and cracks under zero and peak loading from the XCT test and the simulation. A very high level of similarity can be seen in the crack patterns, both on the surface and the interior, indicating the capability of the developed image-based model in predicting the phenomenological damage and fracture processes qualitatively.

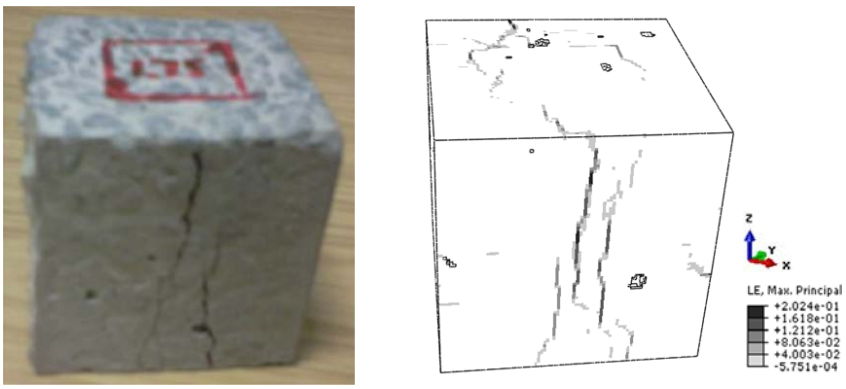

Figure 6. Crack patterns: XCT test (left) and numerical results (right)

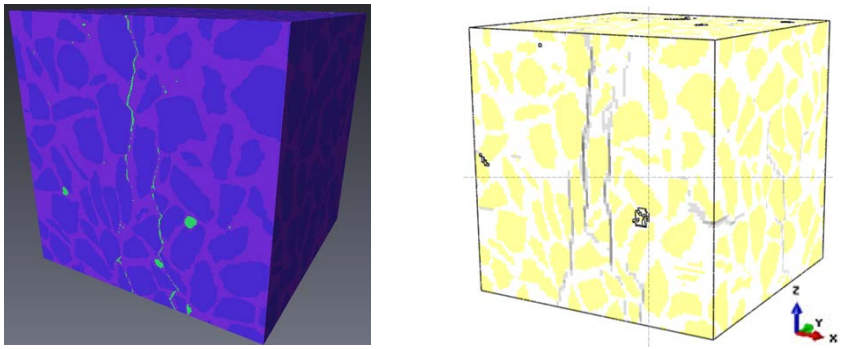

Figure 7. Crack paths: XCT test (left) and numerical results (right)

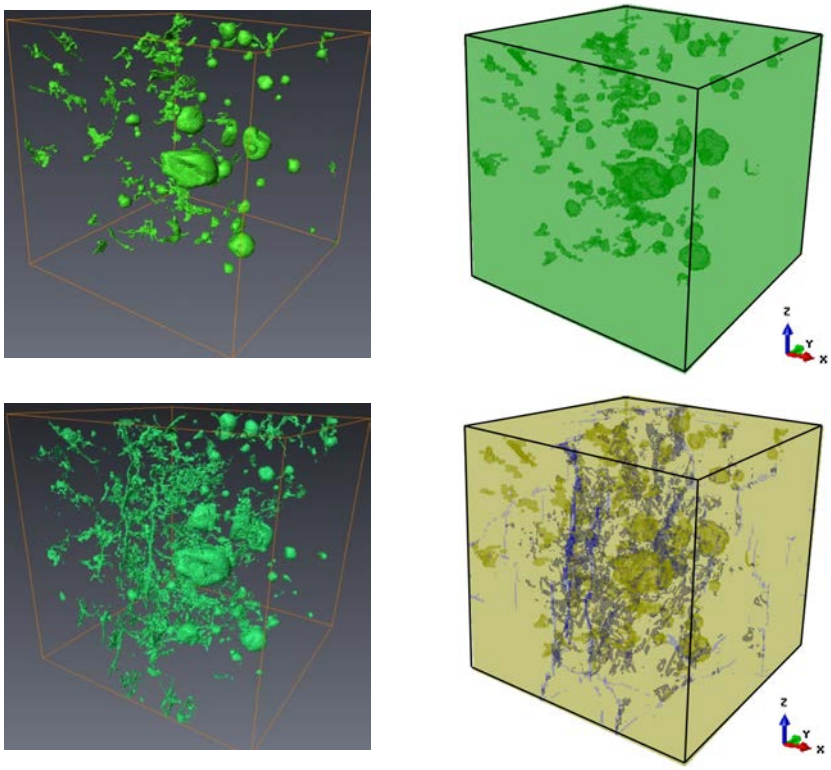

Figure 8. Voids and cracks at zero load stage (top) and peak load (bottom): XCT test (left) and numerical results (right)

More detailed comparison can be made for each slice/cross-section inside the specimen. An example of the middle slice vertical to the loading direction (*z*) at peak load is given in Figure 9. Figure 9a shows the original XCT image and Figure 9b highlights the crack pattern identified by comparing Figure 9a with the image at zero load. Figure 9c and 9d show the predicted maximum principal strain contours from this study and a digital volume correlation (DVC) analysis [Yang et al. (2013)]. A sound resemblance in the crack patterns can be observed.

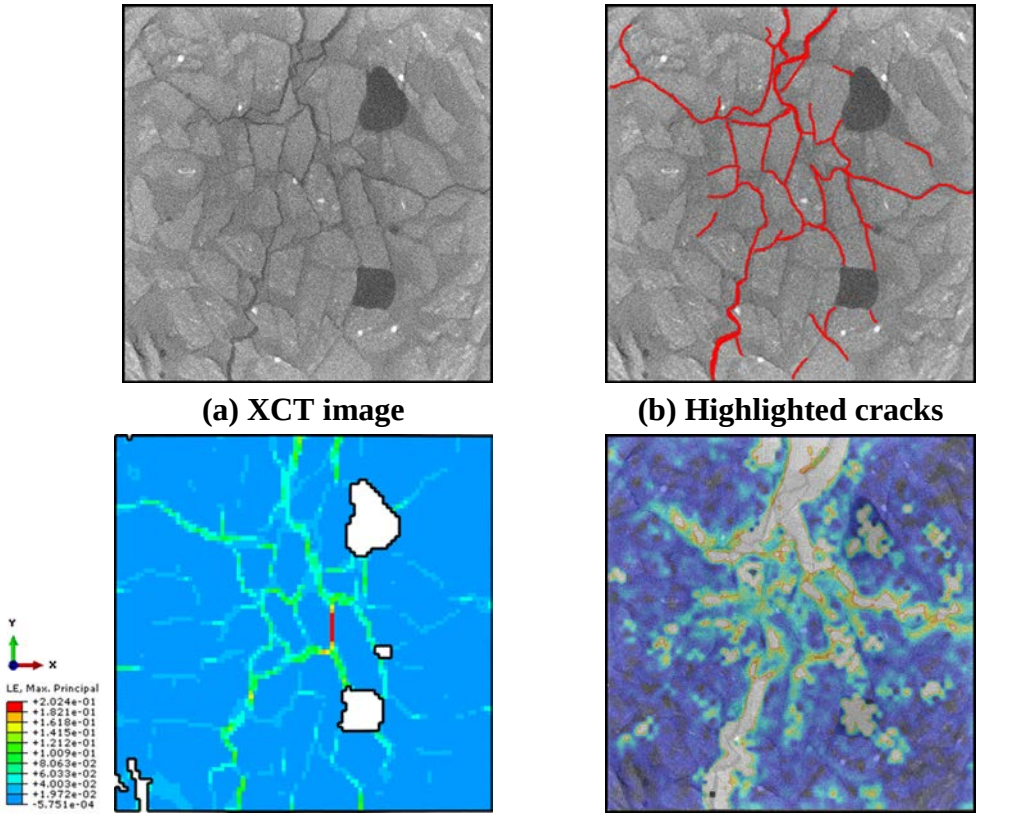

(a) XCT image **(b) Highlighted cracks**

(c) Present simulation **(d) DVC results [Yang et al, (2013)]**

Figure 9. Crack patterns on a slice vertical to the loading at peak load: XCT images (top), numerical results (bottom left) and DVC results (bottom right)

3.4 Further uniaxial compression tests

The same FE model in Figure 5b is used to simulate the uniaxial compression tests, with one entire surface loaded and the opposite fixed vertically without lateral friction. Loading in three directions (x, y and z) is modelled to investigate the effects of multiphase distribution. The predicted stress-strain curves are shown in Figure 10, with key points (A-E) marked. The stress-volumetric strain curves are presented in Figure 11. The different stages in these curves agree well with the typical behaviour of concrete under uniaxial compression [Van Mier (2012)]. The predicted strength is 31.0MPa, 29.0MPa and 28.2MPa for x-load, y-load and z-load respectively, with 9% maximum difference. This together with different post-peak curves indicates the multi-phase distribution at meso-scale affects the macro-scale structural responses. The volumetric strain (Figure 11) decreases first and then increases, reflecting that the specimen becomes more compact under compression first and then expanded after cracks initiate and propagate at late stage. This is also confirmed by the variation of void and crack volume fractions in the XCT test [Yang et al. (2013)].

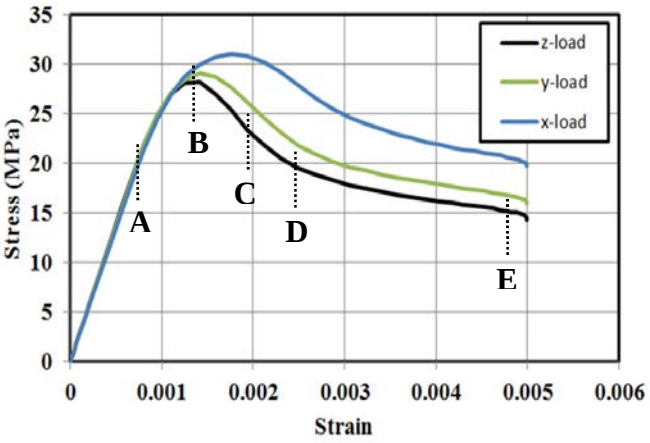

Figure 10. Simulated stress-strain curves for uniaxial compression

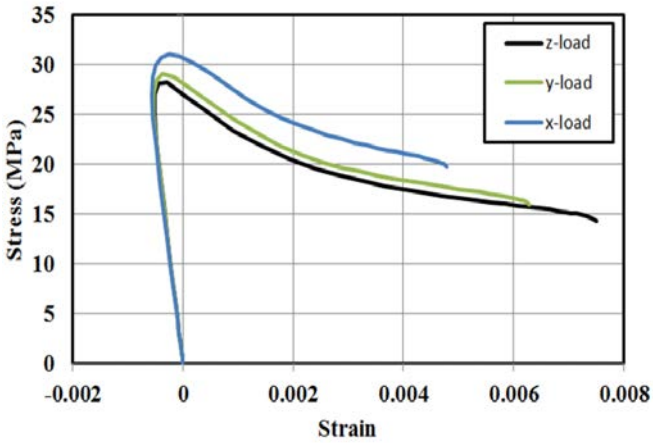

Figure 11. Simulated stress-volumetric strain curves for uniaxial compression

Figure 12 shows the initiation and evolution of compressive damage index (DAMAGEC in ABAQUS) on the surfaces in the front and rear views. The simulated failure pattern with inclined cracks (displayed in red with high damage index) shows similar features to 2D numerical results [Song and Lu (2012)] and typical tests with low friction [Van Mier and Vonk (1991)]. The very different pictures on the front and rear views reflect the heterogeneous mechanical properties caused by random distribution of phases.

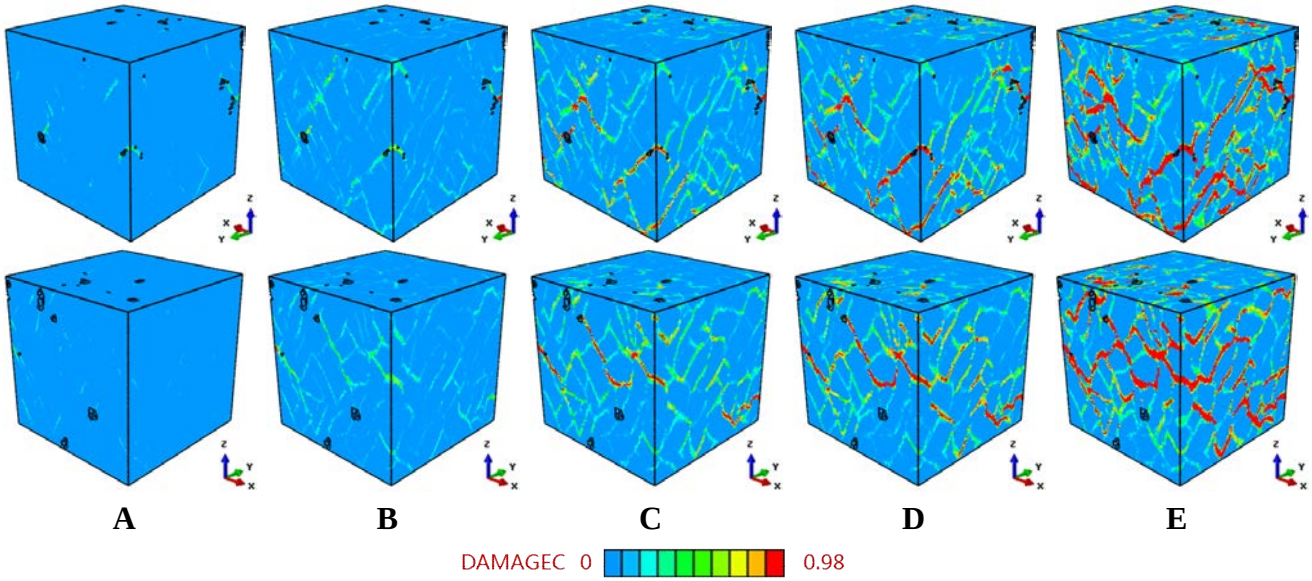

Figure 12. Damage initiation and evolution under z-load at loading points A-E: front view (top) and rear view (bottom)

The internal damage initiation and evolution in a 3D cut-off view (Figure 13) of the model is shown in Figure 14. The view cut is selected to show how the voids and aggregates affect initiation and propagation of damage. From Figure 12 and Figure 14, it can be seen that the damage initiates mostly around the voids. The damage bands tend to propagate towards nearby voids to form a connected 3D damage network with complicated crack bridging and branching. In some cases, the propagation of damage bands is slowed down or hindered by big aggregates (refer to the red arrow in Figure 13) on the way. It can also be noted that the damage and fracture appears to propagate from the surfaces to the interior.

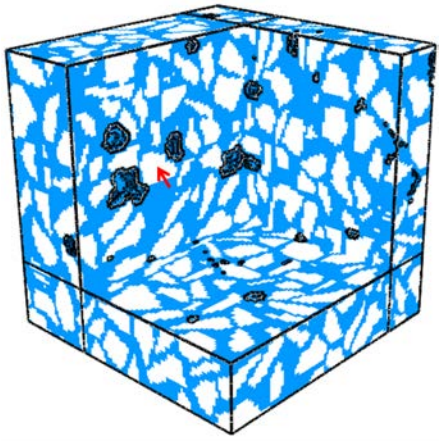

Figure 13. A cut-off view showing main voids

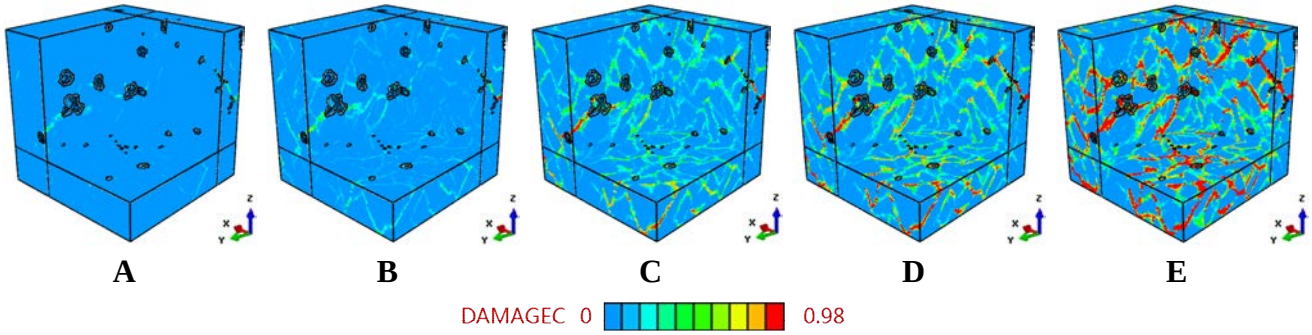

Figure 14. Damage initiation and evolution under z-load at loading points A-E

Figure 15 compares the damage patterns externally and internally at loading point E (Figure 10) from different loading directions. The very different pictures demonstrate that the loading direction, or equivalently, the distribution of phases, can make significant differences to the failure pattern as well as the load-carrying capacities.

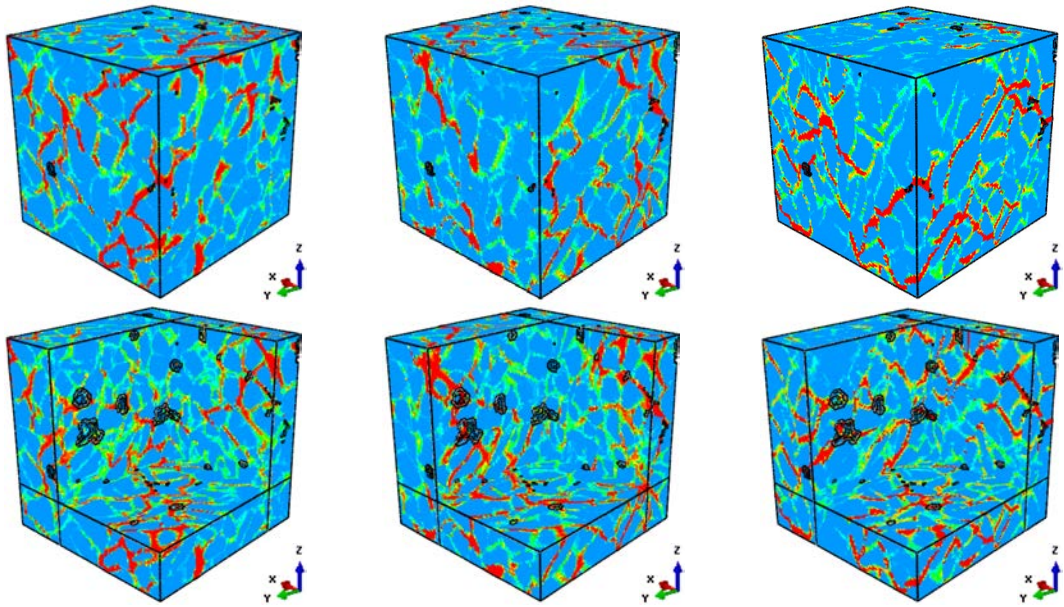

(a) x-load **(b) y-load** **(c) z-load**

Figure 15. Failure patterns under different loading directions

4. Conclusions

3D meso-scale FE models based on XCT images have been developed for accurate understanding of damage initiation and evolution until structural failure of concrete under compression, using the voxel hexahedron meshing method and the concrete damage plasticity model. An attempt to validate the developed models has been made against an in-situ XCT test for the first time, although still phenomenologically and qualitatively in terms of 3D damage and fracture processes.

The numerical results clearly show that the intrinsic heterogeneity of meso-structures caused by random spatial distribution of multi-phases can significantly affect macroscopic responses of concrete, e.g., crack patterns and load-carrying capacities. Moreover, the image-based 3D models are very powerful and promising in elucidating the fundamental mechanism of very complicated damage initiation and propagation behaviour that 2D studies are incapable of modelling.

Acknowledgements

This research is financially supported by National Basic Research Program of China (973 Program Project 2013CB035901), EPSRC UK (No. EP/J019763/1) and the Alexander von Humboldt Foundation, Germany for a Fellowship for Experienced Researchers.

References

Caballero, A., López, C. M., and Carol, I. (2006) 3D meso-structural analysis of concrete specimens under uniaxial tension. *Computer Methods in Applied Mechanics and Engineering*, 195(52), 7182-7195.

Canton, B. and Gilchrist, M. D. (2010) Automated hexahedral mesh generation of complex biological objects: dedicated to the memory of Professor Bertram Broberg, colleague and friend. *Strength, Fracture and Complexity*, 6(1), 51-68.

Chen, G. M., Chen, J. F. and Teng, J. G. (2012) On the finite element modelling of RC beams shear strengthened with FRP. *Construction and Building Materials* 2012;32:13–26.

Crawford, R. P., Keaveny, T. M. and Rosenberg, W. S. (2003) Quantitative computed tomography-based finite element models of the human lumbar vertebral body: effect of element size on stiffness, damage, and fracture strength predictions. *Journal of biomechanical engineering*, 125(4), 434-438.

Hollister, S. J. and Kikuchi, N. (1994) Homogenization theory and digital imaging: a basis for studying the mechanics and design principles of bone tissue. *Biotechnology and Bioengineering*, 43(7), 586-596.

Huang, M., and Li, Y. M. (2013) X-ray tomography image-based reconstruction of microstructural finite element mesh models for heterogeneous materials. *Computational Materials Science*, 67, 63-72.

Keyak, J. H., Fourkas, M. G., Meagher, J. M. and Skinner, H. B. (1993) Validation of an automated method of three-dimensional finite element modelling of bone. *Journal of Biomedical Engineering*, 15(6), 505-509.

Lee, J., and Fenves, G. L. (1998) Plastic-damage model for cyclic loading of concrete structures. *Journal of Engineering Mechanics*, 124(8), 892-900.

López, C. M., Carol, I., and Aguado, A. (2008) Meso-structural study of concrete fracture using interface elements. II: compression, biaxial and Brazilian test. *Materials and Structures*, 41(3), 601-620.

Lubliner, J., Oliver, J., Oller, S., and Oñate, E. (1989) A plastic-damage model for concrete. *International Journal of Solids and Structures*, 25(3), 299-326.

Mahmud, G. H., Yang, Z. J., Hassan, A. (2013) Experimental and numerical studies of size effects of Ultra High Performance Steel Fibre Reinforced Concrete (UHPFRC) beams, *Construction and Building Materials*, Vol. 48, 1027-1034.

Mishnaevsky Jr, L. L. (2005) Automatic voxel-based generation of 3D microstructural FE models and its application to the damage analysis of composites. *Materials Science and Engineering*: A, 407(1), 11-23.

Ren, W. Y., Yang, Z. J. and Sharma, R. (2014) 3D meso-scale image-based fracture modelling of concrete using cohesive elements. *22nd UK National Conference on Computational Mechanics in Engineering*. Exeter, April 2014.

Ren, W. Y., Yang, Z. J. and Withers, P. (2013) Meso-scale fracture modelling of concrete based on X-ray computed tomography images. *The 5th Asia-Pacific Congress on Computational Mechanics (APCOM)*, 11-14th December, 2013, Singapore.

Sharma, R., Ren, W. Y. and Yang, Z. J. (2014) Homogeneous response of random structured concrete with realistic microstructure. *22nd UK National Conference on Computational Mechanics in Engineering*. Exeter, April 2014.

Song, Z., and Lu, Y. (2012) Mesoscopic analysis of concrete under excessively high strain rate compression

Su, X. T., Yang, Z. J. and Liu, G. H. (2010) Monte Carlo simulation of complex cohesive fracture in random heterogeneous quasi-brittle materials: A 3D study. *International Journal of Solids and Structures*, 47:2336-2345.

Terada, K., Miura T. and Kikuchi N. (1997) Digital image-based modelling applied to the homogenization analysis of composite materials. *Computational Mechanics,* 20(4): 331-346.

Van Mier, J. G. M (2012). Concrete Fracture: A Multiscale Approach. *CRC Press.*

Van Mier, J. G. M. and Vonk, R. A. (1991) Fracture of concrete under multiaxial stress-recent developments. *Materials and Structures*, 24(1), 61-65.

Wang, L. B., Frost, J. D. and Voyjadjis, G. Z. (2003) Quantification of damage parameters using X-ray tomography images. *Mechanics of Materials,* 35: 777-790.

Yang, Z. J., and Frank Xu, X. (2008) A heterogeneous cohesive model for quasi-brittle materials considering spatially varying random fracture properties. *Computer methods in applied mechanics and engineering*, 197(45), 4027-4039.

Yang, Z. J., Ren, W. Y., Mostafavi, M., Mcdonald, S. A. and Marrow, T. J. (2013) Characterisation of 3D fracture evolution in concrete using in-situ x-ray computed tomography testing and digital volume correlation. *VIII International Conference on Fracture Mechanics of Concrete and Concrete Structures*, Toledo, Spain, CIMNE.

Yang, Z. J., Su, X. T., Chen, J. F. and Liu, G. H. (2009) Monte Carlo simulation of complex cohesive fracture in random heterogeneous quasi-brittle materials. *International Journal of Solids and Structures*, 46(17): 3222-3234.

Young, P. G., Beresford-West, T. B. H., et al. (2008) An efficient approach to converting three-dimensional image data into highly accurate computational models. Philosophical Transactions of the Royal Society A: *Mathematical, Physical and Engineering Sciences*, 366(1878), 3155-3173.